Self-regulated viscous channel in the nuclear pore complex

Jiong Ma, Alexander Goryaynov, Ashapurna Sarma, and Weidong Yang[1]

Department of Biological Sciences, Center for Photochemical Sciences, Bowling Green State University, Bowling Green, OH 43403

Edited by Thoru Pederson, University of Massachusetts Medical School, Worcester, MA, and accepted by the Editorial Board March 13, 2012 (received for review February 2, 2012)

The nuclear pore complex (NPC), the sole gateway for nucleocytoplasmic exchange in eukaryotic cells, allows for the passive diffusion of small molecules and transport-receptor-facilitated translocation of signal-dependent cargo molecules. Whether small molecules passively diffuse through a single central channel or through multiple holes of a hydrogel network is a subject of debate. Additionally, whether the passive and facilitated transport systems occupy distinct or overlapping physical regions of the NPC remains unclear. Here, we directly test these models using three-dimensional super-resolution fluorescence microscopy of human cells. This approach reveals that a single viscous central channel in the NPC acts as the sole pathway for passive diffusion of various small molecules; transport receptors and their cargo complexes take distinct transport routes in the periphery, which is occluded by phenylalanine-glycine filaments. Furthermore, the passive and facilitated passageways in the NPC are closely correlated, and their conformations can be simultaneously regulated by Importin β1 (a major transport receptor) and RanGTP (a critical regulator of transport directionality). These results strongly favor a self-regulated viscous channel configuration in native NPCs over the porous hydrogel meshwork model.

3D imaging | nucleoporins | single-molecule fluorescence | super-resolution microscopy

The nuclear pore complex (NPC) that is embedded in the nuclear envelope (NE) functions as a highly selective gateway for an exchange of macromolecules between the cytoplasm and nucleus of eukaryotic cells. The NPC is a large assembly of approximately 30 different proteins, known as nucleoporins (Nups), with each present in an integer multiple of eight copies (1–3). Approximately one-third of the total Nups possess a "natively unfolded" structure with domains that are rich in phenylalanine-glycine (FG) repeats. These FG-Nups form the selective permeability barrier in the NPC that allows for two transport modes: passive diffusion of small molecules (<40–60 kDa) and transport-receptor-facilitated translocation of cargo molecules containing specific signals (4, 5). The existence of facilitated translocation suggests that a cargo molecule would be repelled by the NPC unless it is chaperoned by transport receptors (6–8). The dissociation and association of transport-receptor-cargo complexes are guided by a concentration gradient of RanGTP (or RanGDP) across the NE (9, 10). In contrast, the passive diffusion through the NPC requires no consumption of chemical energy.

Electron microscopy studies have revealed that the central nuclear pore is approximately 40–90 nm in length, with a minimum internal diameter of around 40–75 nm and an external diameter of approximately 120 nm. Flexible filaments extend approximately 50 nm into the cytoplasm, and a basket structure extends approximately 75 nm into the nucleus (5, 11). Thus, a transiting substrate can potentially interact continuously with Nups over a distance spanning approximately 200 nm. Nonetheless, due to our limited knowledge of the native configuration of the FG-Nup barrier and of the interactions of the transiting molecules with this barrier, the precise nucleocytoplasmic transport mechanism remains unclear (12–18).

Numerous models for this mechanism have been proposed, and these models make different but testable predictions for passive and facilitated transport. The "oil-spaghetti" and the "reduction of dimensionality" (ROD) models (12, 13) predict that an axial central channel (approximately 10–15 nm in diameter) exists in the NPC and acts as the primary passageway for the passive diffusion of small molecules (Fig. 1*A*). The above-mentioned models, as well as the "virtual gating" and the "polymer brush" models, predict that the binding of transport receptors to FG repeats would promote efficient facilitated translocation of macromolecules by overcoming the entropic barrier of the NPC (2), collapsing FG filaments toward their anchors (12, 14), or conducting two-dimensional (2D) movements on the FG-repeat-coated inner wall of the NPC (13), respectively. In contrast, the "selective phase/hydrogel" model proposes that weak hydrophobic interactions between FG repeats create a sieve-like hydrogel meshwork within the NPC (15, 16, 18) and that small molecules passively diffuse through numerous randomly distributed small holes ($\leq$2.6 nm in diameter) in this mesh (Fig. 1*B*). In this model, transport receptors and their cargo complexes gain efficient translocation through the NPC by dissolving into the FG-hydrogel network rather than by collapsing the FG filaments toward their anchors. Lastly, the "forest" model posits that two separate transport zones could form in the NPC for either passive diffusion or facilitated transport, depending on interactions between FG domains (17).

To distinguish between these models and directly study the mechanism of transport, we developed a single-molecule fluorescence imaging approach, called single-point edge-excitation subdiffraction (SPEED) microscopy (19), and used this technology to observe both passive diffusion and facilitated translocation through native NPCs in three dimensions. This technique allows us to map the 3D configurations of these two transport routes through the FG-Nup barrier in intact, submicrometer NPCs under real-time trafficking conditions, with an unprecedented temporal resolution of 400 μs and a spatial localization accuracy of 9 nm. Specifically, we acquired single-molecule measurements of nucleocytoplasmic transport by adding 1 nM dye-labeled substrates to the NPCs with green fluorescence protein (GFP)-conjugated-POM121 (a Nup anchored in the central scaffold of NPC) in digitonin-permeabilized HeLa cells under reconstructed functional transport conditions (19). SPEED microscopy enabled us to capture a single fluorescent NPC using an inclined diffraction-limited illumination volume in a single cell (Fig. 1*C*). We determined real-time transport times and recorded 2D single-

Author contributions: J.M. and W.Y. designed research; J.M. and W.Y. performed research; J.M., A.G., A.S., and W.Y. analyzed data; and W.Y. wrote the paper.

The authors declare no conflict of interest.

This article is a PNAS Direct Submission. T.P. is a guest editor invited by the Editorial Board.

Freely available online through the PNAS open access option.

[1]To whom correspondence should be addressed. E-mail: wyang@bgsu.edu.

This article contains supporting information online at www.pnas.org/lookup/suppl/doi:10.1073/pnas.1201724109/-/DCSupplemental.

Downloaded by guest on February 24, 2022

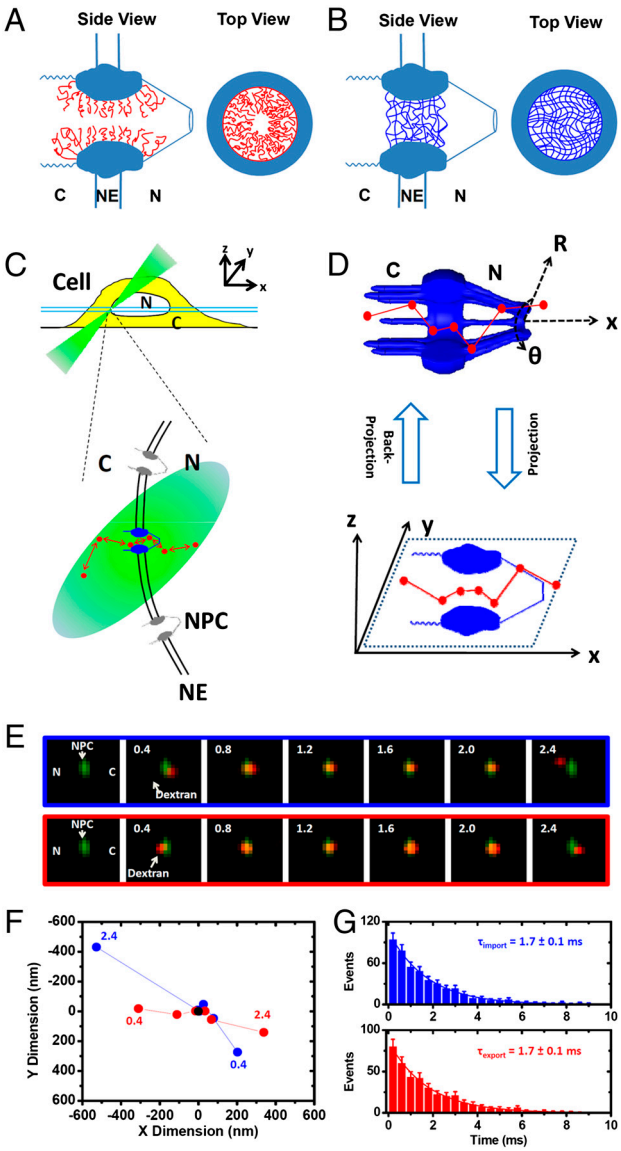

Fig. 1. Nucleocytoplasmic transport models and experimental design. (*A*) A single-channel schematic is shown in both a side view and a top view. The filaments of Nups (red curves) form a physical or entropic barrier for large molecules and leave a narrow axial central channel for small molecules in the NPC. (*B*) The "selective phase/hydrogel" model. Hydrophobic interactions between the FG repeats generate a sieve-like hydrogel meshwork (blue mesh). C, the cytoplasmic side of the NPC; NE, nuclear envelope; N, the nucleoplasmic side of the NPC. (*C*) Illumination of a single NPC in a cell by SPEED microscopy. Single transiting molecules (red dots) through a single GFP-NPC (blue) are imaged using an inclined illumination point spread function (iPSF forms an angle of 45° to the z direction) at the equatorial plane of a HeLa cell nucleus in the focal plane (between the double light blue lines). C, cytoplasm; N, nucleus. (*D*) The 2D to 3D deconvolution process. Using deconvolution algorithms (19), the 3D spatial locations of transiting molecules in the NPC in a cylindrical coordinate system (R, θ, x) are recovered from the obtained 2D spatial locations in the xy plane. (*E–G*) Single-molecule trajectories and transport times through single NPCs. Typical nucleocytoplasmic import and export events of transiting molecules (red spots) through a single GFP-NPC (green spot) and their trajectories (blue dots for import, red for export and black for the centroid of the NPC) are shown in *E* and *F*. Numbers denote a series of frames, noting time in milliseconds. The import or export time of approximately 1.7 ms for the 10 kDa dextran is determined from a monoexponential decay function as shown in *G*.

molecule tracking trajectories of molecules transiting through the illuminated NPCs (Fig. 1 *E–G* and Fig. S1, Table S1, and Movies S1–S5). The 2D probability density maps of single-molecule tracking trajectories were then converted into the corresponding 3D probability density maps in the NPC using a deconvolution algorithm (19) (Fig. 1*D*).

Results and Discussion

Three-Dimensional Spatial Probability Density Maps of Passive and Facilitated Transport in the NPC. Fluorescent transiting substrates of different sizes (0.3–217 kDa in molecular weight, approximately 1.4–12.8 nm in diameter), including organic dyes, dextrans, proteins, transport receptor Imp β1, and the model import cargo complex Imp α/Imp β1/NLS-2xGFP (nuclear localization sequence of PPKKKRKV linked to a GFP dimer), were tracked through single native NPCs. Extensive control experiments have shown that labeled dyes do not alter functional nucleocytoplasmic transport of transport receptors and their cargo complexes (19, 20–23). In 10 NPCs of 10 cells, 1,500 to 5,000 spatial locations for each substrate were collected from 110–750 single-molecule nucleocytoplasmic transport events (Fig. 2).

The 3D probability spatial distributions of transiting molecules recovered from their 2D probability density maps demonstrate that small molecules (0.3–29 kDa) smoothly diffuse through a single axial central channel in the native NPCs (Fig. 2 *A–G* and Movie S6). This central channel was found to be less permeable for the 41 kDa dextran molecules and almost completely impermeable to the 61 kDa GFP dimers and 72 kDa dextran molecules (Fig. 2 *H–J*). Our measured cut-off size of approximately 40–60 kDa for passive diffusion through the NPC is consistent with previously obtained data from electron micrographs or estimations of size from measurements of bulk transport rates (1, 5, 15). The transport receptor Imp β1 and the import cargo complexes, which have even larger sizes and interact with FG-Nups, were observed to efficiently transport through the NPC, but these molecules were mainly found in the periphery and seldom in the central channel (Fig. 2 *K* and *L*). The existence of distinct passageways for passive and facilitated transport was confirmed by examining the spatial distributions of 10 kDa dextran and Imp β1 molecules in cross-sections of the illuminated single NPCs at the bottom of the NE (Fig. S2). Moreover, other transport receptors, such as NTF2 and transportin (also known as Imp β2), were also found to transport through the peripheral region around the Imp β1-unoccupied single axial tube in native NPCs (Fig. S3).

Thus, our data show that (*i*) a single central channel serves as the major pathway for the passive diffusion of various small molecules, and (*ii*) our method allows for recording of the 3D spatial configurations of the central passive diffusion route and the peripheral facilitated transport pathways under real-time trafficking conditions in native NPCs. Our results strongly support the existence of a single-channel configuration in the NPC, as proposed in the oil-spaghetti and the ROD models (12, 13), and do not support the existence of multiple holes in a hydrogel meshwork, as proposed by the selective phase/hydrogel model (15, 16). This conclusion is consistent with previous statements that have been made to suggest that passive and active transport the NPCs occurs via distinct paths (24, 25) as well as with the prediction of double transport zones by the forest model (17).

Distinct but not Completely Separate Passive and Facilitated Transport Zones. Previous controversial experimental results have fueled a debate over the spatial and functional overlap between passive and facilitated modes of transport (24–28). In our measurements, compared to cargo-free Imp β1, the import cargo complex pervaded more into the central passive diffusion pathway (the diameter of the Imp β1-unoccupied central channel in the middle plane of the NPC was found to be 23 ± 3 nm with cargo-free Imp β1 and only 8 ± 4 nm with cargo-bound Imp β1, Fig. 2 *K* and *L*). The differences between the paths of cargo-free and cargo-bound Imp β1 have been previously attributed to the size of the cargo complex and the orientation of labeled cargo in the cargo com-

BIOPHYSICS AND COMPUTATIONAL BIOLOGY

Downloaded by guest on February 24, 2022

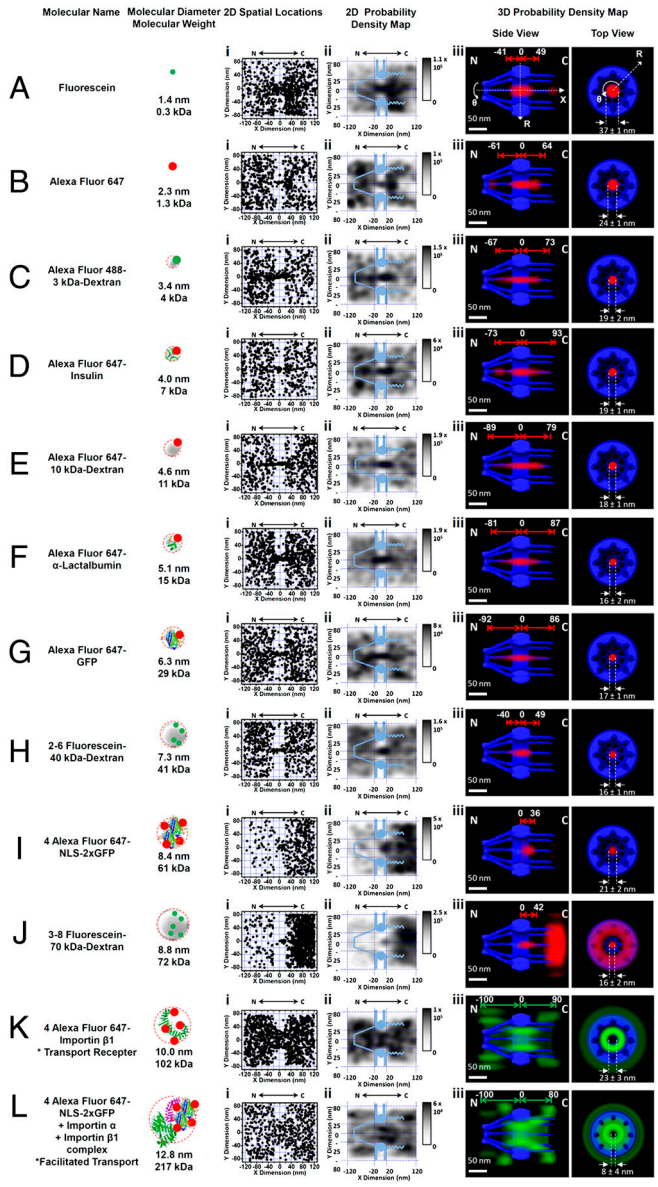

Fig. 2. Two-dimensional superimposed spatial locations and three-dimensional probability density maps for various fluorescent transiting substrates. (*A*) Fluorescein dye. Superimposed plots of spatial localizations of single fluorescein molecules located primarily within a rectangular area of 240 × 160 nm around the centroid of the NPC (i). The locations in each 10 × 10 nm area were quantized and filtered with a Gaussian blur function to generate the 2D probability density map overlaid onto the NPC architecture (light blue). The highest density was 1.1×10^5 locations/μm^2 and the lowest was 0 locations/μm^2, as shown in gray (ii). A 3D probability density map was generated using a 2D to 3D deconvolution (19) (red cloud; brighter color indicates higher density) and is shown in both side-view and a top-view orientations superimposed on the NPC architecture (blue). The distance from the NPC centroid and the diameter at the central plane of NPC were measured (iii). N, the nucleoplasmic side of the NPC. C, the cytoplasmic side of the NPC. (*B–J*) Passive diffusion of fluorescent substrates with different sizes through the NPC. (*K*) Labeled Imp β1. The 3D probability density map is shown as a green cloud, in which the brighter color indicates a higher density. (*L*) Labeled NLS-2xGFP forming an import complex with Imp α and Imp β1.

plex (19). Larger receptor-cargo complexes can inhabit more space in the passive diffusion channel. Small molecules were also found to invade the peripheral FG filamentous regions in both the axial and the radial directions of the NPC (Fig. 3); the partition depth strongly depended on the molecular size. As illustrated by the superimposed routes of passive diffusion of small molecules and cargo-free or cargo-bound Imp β1 (Fig. 3 *A–D* and Fig. S4 and Movies S7–S8), 0.3 kDa fluorescein molecules diffuse much deeper into the FG-repeat-Imp β1 interacting domains than 29 kDa GFP molecules in all five distinct interaction regions. Quantitatively, the length and the central diameter of the passive diffusion paths (based on the e^{-2} width of Gaussian fit) were found to change from 140–179 nm and 17–19 nm for larger passively diffusing molecules (approximately 3–7 nm in diameter) to 88–125 nm and 24–37 nm for smaller molecules (< ∼ 3 nm in diameter), respectively (Fig. 3*D* and Table S2). The above data clearly indicate that the larger the facilitated transport cargo complex or the smaller the passively diffusing molecule, the bigger the overlapping areas between passive and facilitated passageways. Therefore, these two distinct transport zones in the NPC are not completely separate from one another, and the extent of overlap between them strongly depends on the molecular sizes of the transiting substrates.

A Single Viscous Central Channel in the NPC. Another point of disagreement in the existing models is the question of whether the central channel is an open aqueous conduit. With SPEED microscopy, we measured the diffusion time (τ) of small molecules transiting through the NPC by determining their dwell time based on their single-molecule tracking trajectories (as τ in Fig. 1*G*). Having determined the dimensions of the central passive diffusion channel for each small molecule, we could calculate a theoretical diffusion time for the small molecules (t) using the equation $t = \frac{\langle \delta^2_{\text{axis}}(t) \rangle}{2A_c D_{\text{axis}}}$, where $\delta_{\text{axis}}(t)$ is the instantaneous moving distance of a small molecule projected along the axis of the NPC, $\langle \delta^2_{\text{axis}}(t) \rangle$ is the length of the central channel measured for the small molecule, A_c is the spatial confinement effect exerted by the nuclear pore on inserted molecules (29). $D_{\text{axis}} (= \frac{KT}{6\pi r \eta_{\text{aqueous}}})$ is the projected diffusion coefficient of the substrates transiting through an aqueous channel along the NPC axis, in which η_{aqueous}, K, T, and r correspond to the viscosity in an open aqueous channel ($\eta_{\text{aqueous}} = 1$ cP), the Boltzman constant, temperature, and the molecular radius, respectively. As shown in Fig. 3*E*, the transport times measured for various small molecules in the NPC are much longer than those that were calculated for small molecules passively diffusing through an open aqueous channel, making it unlikely that an aqueous open central channel exists in native NPCs.

The effective viscosity ($\eta_{\text{pore}} = \frac{\tau}{t} * \eta_{\text{aqueous}}$) of the medium in the central channel of a native NPC was found to vary from 1.6 cP (for molecules = ∼3–7 nm in diameter) to 3.4 cP (for molecules < ∼ 3 nm in diameter) (Fig. 3*F*). What underlies this high viscosity? The central passive diffusion route is surrounded by filaments of FG Nups that interact with transport receptors (Fig. 3*B*). Some FG filaments are predicted to be long enough to protrude into the central channel (16, 17). While transport receptors mostly interact with FG filaments at the periphery and are seldom located in the central tube, the density of FG filaments in the channel would be much lower than in the peripheral region. These sparse and extended FG filaments in the central channel could affect passively diffusing molecules, generating a more viscous environment and increasing the diffusion time for small molecules. Very small molecules (< ∼ 3 nm in diameter) that are capable of reaching even further into the peripheral filamentous regions would encounter crowded FG filaments, which could certainly generate a more viscous microenvironment (Fig. 3*F*). In summary, the above measurements suggest that a single central channel filled with a complex, inhomogeneous and viscous medium, rather than an open aqueous conduit, exists in the native NPC.

The Conformations of Passive and Facilitated Passageways in the NPC Regulated by Imp β1 and RanGTP. We next sought to determine

Downloaded by guest on February 24, 2022

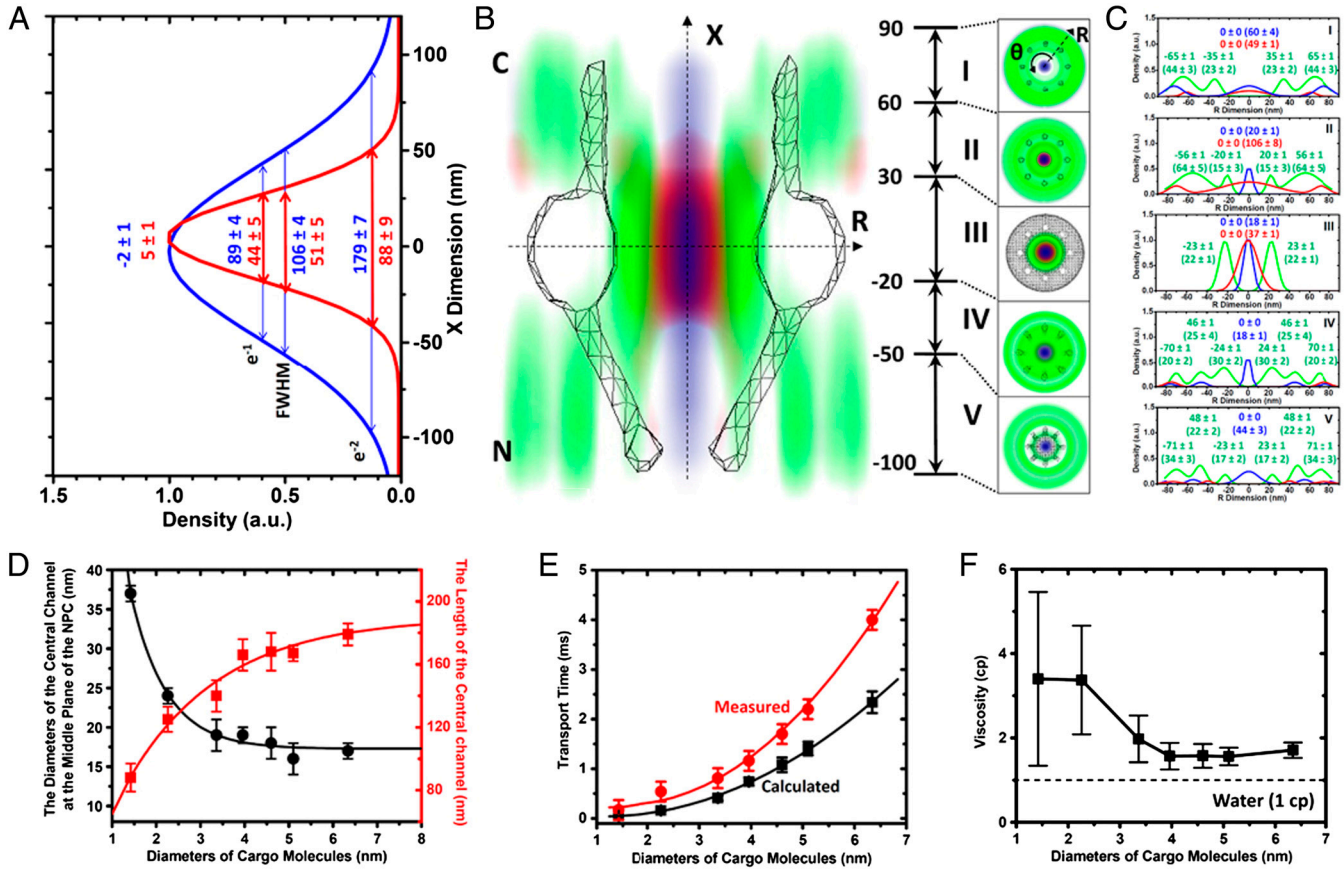

Fig. 3. Superimposed transport routes of passive diffusion and facilitated translocation and the effective viscosity of the medium in the central passive diffusion channel. (*A*) Length of passive diffusion channel in the NPC obtained from the e^{-1}, FWHM, and e^{-2} widths of the Gaussian fits of the probability densities of 0.3 kDa fluorescein (red) and 29 kDa GFP (blue) along the X direction. (*B*) Central slice along the nucleocytoplasmic axis of the 3D probability density maps of Imp β1 (green cloud), 0.3 kDa fluorescein (red), and GFP (blue), superimposed onto the NPC structure (gray sketch). The cross-sections along the R dimension in five distinct regions are marked from I to V with relative distances from the centroid of the NPC. All distances are in nanometers. C, the cytoplasmic side of NPC. N, the nucleoplasmic side of NPC. (*C*) Histograms of spatial probability densities for the above three transiting molecules along the radii (R) at the cross-section of NPC in ranges I to V. Major peaks and e^{-2} widths (in brackets) for Imp β1 (green), fluorescein (red) and GFP (blue) were obtained from Gaussian fittings. (*D*) The length and diameter of the passive diffusion channel as a function of the molecular sizes of transiting molecules. (*E*) Comparisons between measured (red) and calculated (black, assuming a viscosity of 1*cP*) nucleocytoplasmic diffusion times for molecules of different sizes. (*F*) Effective viscosity of the medium in the central channel for each substrate.

whether Imp β1 could alter the conformations of FG-Nup filaments in the native NPC and thereby modify the dimensions of the passive and active transport pathways. In vitro experiments have shown that 33 nM Imp β1 molecules collapse the FG filaments of Nup153 toward their anchoring sites and that the addition of RanGTP reverses this collapse (14). However, similar measurements conducted on the FG filaments of Nsp1 suggested that there was no collapse (30). Both experiments used a single isolated FG-Nup in vitro. Whether the filaments of FG-Nups could be collapsed by Imp β1 in native NPCs remains an open question. The estimated physiological concentration of Imp β1 in living cells is 3 μM and that of total transport receptors is 15 μM (10, 31). To test whether the conformations of FG filaments and transport routes in native NPCs would be altered by the presence of micromolar concentrations of Imp β1, we performed three types of experiments. In the first experiment, we used Imp β1, which has been reported to interact with the FG repeats of all FG-Nups in the NPC, as a probe to detect the spatial distributions of the available FG repeats in the native NPC under various Imp β1 concentrations (0–15 μM). In the second experiment, we determined the 3D paths of the cargo complexes at different Imp β1 concentrations. In the third experiment, the 3D paths of passive diffusion were obtained at various Imp β1 concentrations.

Using SPEED microscopy, we measured the 3D pathways of 1 nM labeled Imp β1, the import cargo complex or 10 kDa dextran in the presence of 0 μM, 3 μM and 15 μM unlabeled Imp β1 (Fig. 4*A* and Fig. S5, Movies S9 and S10, and *SI Text*). As shown in Fig. 4*A*, the length of the 3D pathway of Imp β1 was found to decrease from 190 ± 5 nm at 1 nM of Imp β1, to 180±5 nm at 3 μM and 160±5 nm at 15 μM. The diameter of the Imp β1-unoccupied channel in the middle plane of the NPC was found to increase from 18±1 nm at 1 nM of Imp β1, to 22±2 nm at 3 μM and 30±2 nm at 15 μM (Fig. 4*C*). Imp β1-regulated conformational changes were also observed for the 3D pathways of the import cargo complexes (Fig. S5). Remarkably, upon measuring the 3D passive diffusion path of 10 kDa dextran molecules in the NPC, we found that the length of the passive diffusion channel was also reduced and the diameter was larger as Imp β1 concentration increased (Fig. 4 *B* and *C*). As both routes were affected by the addition of Imp β1, there appears to be a close correlation between the passive and the facilitated pathways.

In principle, the spatial distribution of the binding sites between FG-Nups and cargo-free or cargo-bound Imp β1 could be changed by (*i*) altered binding affinities between FG repeats and Imp β1 at higher Imp β1 concentrations, (*ii*) Imp β1-concentration-dependent conformational changes in the FG filaments, or (*iii*) a combination of the above. The altered physical dimensions of the central passive diffusion channel observed at different Imp β1 concentrations could not be caused by altered binding affinities between FG-Nups and Imp β1, however, because no

BIOPHYSICS AND COMPUTATIONAL BIOLOGY

Downloaded by guest on February 24, 2022

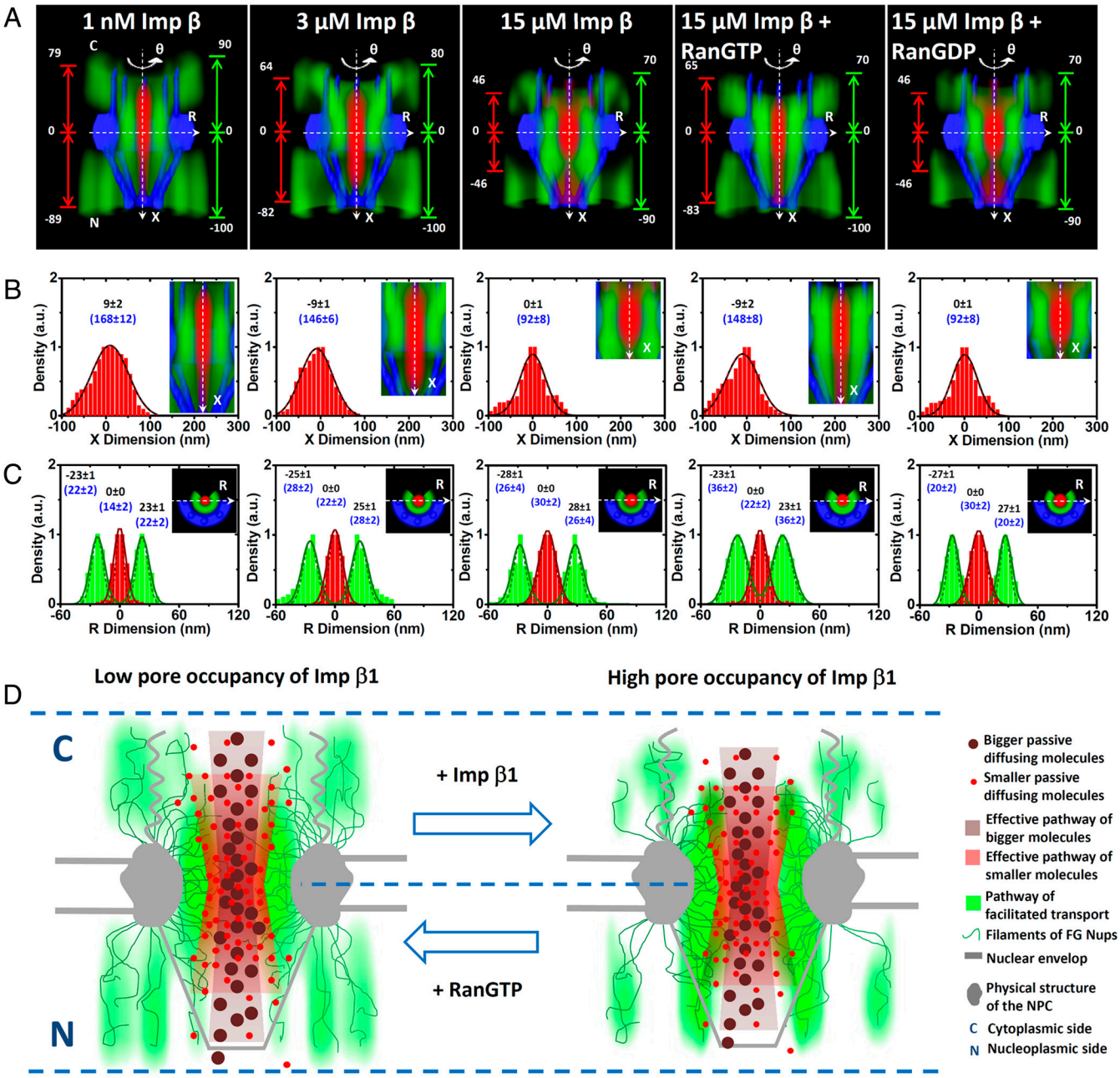

Fig. 4. Three-dimensional pathways of passive and facilitated transport regulated by Imp β1 and RanGTP. (*A*) Cut-away view of the 3D pathways for Imp β1 (green cloud) and dextran (red cloud) superimposed on the NPC architecture (blue) under different experimental conditions. The relative distances from the centroid of the NPC for the pathways of Imp β1 (green) and dextran (red) in the *x* dimension of a cylindrical system (*x*, *R*, *θ*) are shown in nanometers. (*B*) Lengths of pathways for dextran in the *x* dimension (inset, side-view images adapted from *A*). Histogram of the spatial probability density for dextran in the *x* dimension was fitted to a Gaussian function to obtain a major peak and an e^{-2} width (in brackets) under each condition. (*C*) Diameter of the central channel in the *R* dimension under each condition (inset, cross-section images at the middle plane of the 3D probability density maps in *A*). (*D*) A "self-regulated viscous channel" (SERVICE) mechanism. Conformations of the FG barrier in the NPC and the corresponding passageways for the passive diffusion of smaller molecules (red and brown regions), transport receptors and transport-receptor-cargo complexes (green region) strongly depend on the NPC's occupancy of transport receptors. Pore occupancy can be regulated by the number of transport receptors (e.g., Imp β1) interacting with the NPC and the concentration gradient of RanGTP along the NPC.

FG-Nup binding sites are needed for the passive diffusion of small molecules through the NPC. Instead, the conformations of the FG filaments must be altered. Not only did we observe changes in the physical structure, but we also found that the enlarged central passive diffusion channel in the NPC at 15 μM Imp β1 makes the NPC more permeable to the 70 kDa dextran molecules, which generally fail to efficiently diffuse passively through NPCs at 1 nM Imp β1 (Fig. 2 and and Fig. S6).

Remarkably, the Imp β1-dependent conformational changes in the FG filaments can be reversed by the addition of RanGTP (Fig. 4). The conformational changes in the pathways for Imp β1, the import cargo complex and passive diffusion were all found to be reversed when 2 μM RanGTP was added to dissociate Imp β1 from the NPC in the presence of 15 μM Imp β1 (Fig. 4 *A*–*C*). Almost no change was observed for any pathway after the addition of RanGDP, as expected (Fig. 4 *A*–*C*).

Downloaded by guest on February 24, 2022

Lastly, we examined the 3D pathways of cargo-free and cargo-bound Imp β1 in the presence of 15 μM 10 kDa unlabeled dextran molecules and found that a high concentration of small molecules diffusing through the NPC does not alter the conformations of the facilitated pathways.

These results show that the conformations of the FG-Nup filaments that interact with Imp β1 in the NPC are specifically regulated by the amount of Imp β1 and RanGTP in the NPC. The reversible conformational change of some FG-Nups in intact NPCs might correspond to the reversible collapse of the FG-filaments described in the polymer brush model (14).

Conclusions

In summary, we found that a viscous central axial channel serves as the sole passageway for the passive diffusion of small molecules in the NPC, which is consistent with the oil-spaghetti and ROD models for NPC transport (12, 13). Our observations do not support the existence of multiple channels that are randomly distributed in the NPC, as has been proposed by the selective phase/hydrogel model (15, 16, 18). We found that Imp β1 and the import cargo complexes, which mainly interact with the FG repeats on the periphery of the central channel, possess distinct pathways from that of the small molecules. Nonetheless, we found that these two transport routes are not completely spatially separated and that the extent of overlap depends on the molecular sizes of the transiting substrates. This result sheds light on the debate over whether passive and active transport share overlapping or separate spaces in the NPC (24–27). We also found that the 3D conformations of the pathways for both passive and active transport are closely correlated and depend on the amount of Imp β1 that is available to interact with the FG repeats and the concentration gradient of RanGTP along the NPC. This result indicates that a reversible conformational change of the FG-Nup barrier occurs in intact NPCs.

Previous studies have shown similar nucleocytoplasmic transport kinetics for cargo-bound or cargo-free transport receptors in permeabilized and living cells (22, 31). Recently, it was reported that in living cells, each NPC is capable of providing binding sites for up to 100 Imp β1 molecules (approximately 70 μM), and routinely mediating approximately 1000 translocation events, corresponding to a total mass of 10–20 MDa, every second (15, 20–22, 32). The ability of the FG barrier in the NPC to adopt different conformations according to the transport receptors and RanGTP that we have observed here may be crucially important for accomplishing massive, efficient and robust nucleocytoplasmic transport in living cells.

We have summarized the dynamic conformational changes of the FG-Nup barrier and the corresponding regulated distinct transport pathways in the NPC in a model we term "self-regulated viscous channel" (SERVICE). In this model, we propose that compact FG-Nup filaments functioning for transport-receptor-facilitated translocation anchor at the nuclear wall but sparsely permeate the central axial channel for the passive diffusion of small molecules. The conformation of these FG-Nup filaments is dynamically regulated by transport receptors (e.g., Imp β1) and energy regulators (e.g., RanGTP) to meet the needs of the cell for nucleocytoplasmic trafficking (Fig. 4*D*).

Materials and Methods

For these experiments, we used a HeLa cell line stably expressing GFP-POM121. Freshly split cells were grown overnight on coverslips in DMEM supplemented with 10% FBS. For microscopy, flow chambers were constructed using a top coverslip and two lines of silicone grease as spacers. The SPEED microscope includes an Olympus IX81 equipped with a 1.4 NA 100× oil-immersion apochromatic objective (UPLSAPO 100X, Olympus), a 35 mW 633 nm He-Ne laser (Melles Griot), a 120 mW ArKr tunable ion laser (Melles Griot), an on-chip multiplication gain charge-coupled device camera (Cascade 128+, Roper Scientific) and the Slidebook software package (Intelligent Imaging Innovations) for data acquisition and processing. A more detailed explanation of the materials and methods is available in *SI Text*.

ACKNOWLEDGMENTS. We thank S. M. Musser for some plasmids; B. Burke for the GFP-POM121 HeLa cells; and S. M. Musser and M. Rexach for critical comments. The project is supported by the grants of the National Institutes of Health (NIH GM094041 and GM097037).

1. Rout MP, et al. (2000) The yeast nuclear pore complex: composition, architecture, and transport mechanism. *J Cell Biol* 148:635–651.
2. Rout MP, Aitchison JD, Magnasco MO, Chait BT (2003) Virtual gating and nuclear transport: The hole picture. *Trends Cell Biol* 13:622–628.
3. Suntharalingam M, Wente SR (2003) Peering through the Pore. Nuclear pore complex structure, assembly, and function. *Dev Cell* 4:775–789.
4. Fried H, Kutay U (2003) Nucleocytoplasmic transport: Taking an inventory. *Cell Mol Life Sci* 60:1659–1688.
5. Fahrenkrog B, Aebi U (2003) The nuclear pore complex: Nucleocytoplasmic transport and beyond. *Nat Rev Mol Cell Biol* 4:757–766.
6. Bayliss R, Littlewood T, Stewart M (2000) Structural basis for the interaction between FxFG nucleoporin repeats and importin-beta in nuclear trafficking. *Cell* 102:99–108.
7. Bayliss R, Littlewood T, Strawn LA, Wente SR, Stewart M (2002) GLFG and FxFG nucleoporins bind to overlapping sites on importin-beta. *J Biol Chem* 277:50597–50606.
8. Otsuka S, et al. (2008) Individual binding pockets of importin-beta for FG-nucleoporins have different binding properties and different sensitivities to RanGTP. *Proc Natl Acad Sci USA* 105:16101–16106.
9. Rexach M, Blobel G (1995) Protein import into nuclei: Association and dissociation reactions involving transport substrate, transport factors, and nucleoporins. *Cell* 83:683–692.
10. Ribbeck K, Lipowsky G, Ken HM, Stewart M, Gorlich D (1998) NTF2 mediates nuclear import of Ran. *EMBO J* 17:6587–6598.
11. Beck M, et al. (2004) Nuclear pore complex structure and dynamics revealed by cryoelectron tomography. *Science* 306:1387–1390.
12. Macara IG (2001) Transport into and out of the nucleus. *Microbiol Mol Biol Rev* 65:570–594.
13. Peters R (2005) Translocation through the nuclear pore complex: Selectivity and speed by reduction-of-dimensionality. *Traffic* 6:421–427.
14. Lim RY, et al. (2007) Nanomechanical basis of selective gating by the nuclear pore complex. *Science* 318:640–643.
15. Ribbeck K, Gorlich D (2001) Kinetic analysis of translocation through nuclear pore complexes. *EMBO J* 20:1320–1330.
16. Frey S, Gorlich D (2007) A saturated FG-repeat hydrogel can reproduce the permeability properties of nuclear pore complexes. *Cell* 130:512–523.
17. Yamada J, et al. (2010) A bimodal distribution of two distinct categories of intrinsically-disordered structures with separate functions in FG nucleoporins. *Mol Cell Proteomics* 9:2205–2224.
18. Mohr D, Frey S, Fischer T, Guttler T, Gorlich D (2009) Characterization of the passive permeability barrier of nuclear pore complexes. *EMBO J* 28:2541–2553.
19. Ma J, Yang W (2010) Three-dimensional distribution of transient interactions in the nuclear pore complex obtained from single-molecule snapshots. *Proc Natl Acad Sci USA* 107:7305–7310.
20. Yang W, Gelles J, Musser SM (2004) Imaging of single-molecule translocation through nuclear pore complexes. *Proc Natl Acad Sci USA* 101:12887–12892.
21. Yang W, Musser SM (2006) Visualizing single molecules interacting with nuclear pore complexes by narrow-field epifluorescence microscopy. *Methods* 39:316–328.
22. Yang W, Musser SM (2006) Nuclear import time and transport efficiency depend on importin beta concentration. *J Cell Biol* 174:951–961.
23. Sun C, Yang W, Tu LQ, Musser SM (2008) Single molecule measurements of importin alpha/cargo complex dissociation at the nuclear pore. *Proc Natl Acad Sci USA* 105:8613–8618.
24. Naim B, et al. (2007) Passive and facilitated transport in nuclear pore complexes is largely uncoupled. *J Biol Chem* 282:3881–3888.
25. Fiserova J, Richards SA, Wente SR, Goldberg MW (2010) Facilitated transport and diffusion take distinct spatial routes through the nuclear pore complex. *J Cell Sci* 123:2773–2780.
26. Mohr D, Frey S, Fischer T, Guttler T, Gorlich D (2009) Characterization of the passive permeability barrier of nuclear pore complexes. *EMBO J* 28:2541–2553.
27. Hinshaw JE, Carragher BO, Milligan RA (1992) Architecture and design of the nuclear pore complex. *Cell* 69:1133–1141.
28. Herrmann M, et al. (2009) Near-field optical study of protein transport kinetics at a single nuclear pore. *Nano Lett* 9:3330–3336.
29. Cui ST (2005) Molecular self-diffusion in nanoscale cylindrical pores and classical Fick's law predictions. *J Chem Phys* 123:054706.
30. Eisele N, et al. (2010) Ultrathin nucleoporin phenylalanine-glycine repeat films and their interaction with nuclear transport receptors. *EMBO Rep* 11:366–372.
31. Dange T, Grünwald D, Grünwald A, Peters R, Kubitscheck U (2008) Autonomy and robustness of translocation through the nuclear pore complex: A single-molecule study. *J Cell Biol* 183:77–86.
32. Paradise A, Levin MK, Korza G, Carson JH (2007) Significant proportions of nuclear transport proteins with reduced intracellular mobilities resolved by fluorescence correlation spectroscopy. *J Mol Biol* 365:50–65.

Downloaded by guest on February 24, 2022